THE JOURNAL OF PHYSICAL CHEMISTRY A

Article

pubs.acs.org/JPCA

Molecular Excited States: Accurate Calculation of Relative Energies and Electronic Coupling Between Charge Transfer and Non-Charge Transfer States

Brad S. Veldkamp,[†] Xinle Liu,[‡] Michael R. Wasielewski,[†] Joseph E. Subotnik,[‡] and Mark A. Ratner*[,†]

[†]Department of Chemistry and Argonne-Northwestern Solar Energy Research (ANSER) Center, Northwestern University, Evanston, Illinois 60208-3113, United States

[‡]Department of Chemistry, University of Pennsylvania, Philadelphia, Pennsylvania 19104, United States

ABSTRACT: We show for a series of six small donor−acceptor dyads that the energy difference between non-charge transfer (non-CT) and charge transfer (CT) excited states, as well as the squares of the electronic couplings between these states, can be predicted from first-principles using variational orbital adapted configuration interaction singles (VOA-CIS) theory. VOA-CIS correctly predicts the observed experimental trends in these values and provides quantitative accuracy roughly on par with a modern long-range corrected density functional, ωB97X. Using VOA-CIS and ωB97X, the experimental energy difference between the non-CT and CT excited states is predicted with root mean squared errors of 0.22 eV and 0.21 eV, respectively. The square of the electronic coupling between these states is predicted with root mean squared errors of 0.08 eV^2 and 0.07 eV^2, respectively. Orbital optimized CIS (OO-CIS) and CIS(D), two perturbative corrections to CIS, provide a significant correction to the errant relative energies predicted by CIS, but the correction is insufficient to recover the experimentally observed trend.

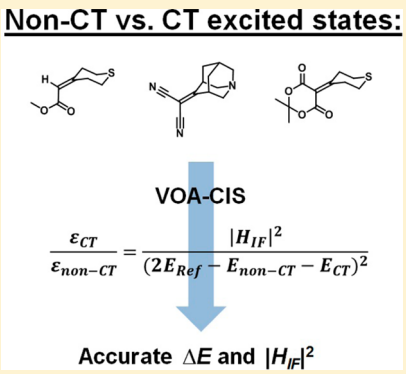

I. INTRODUCTION

Efficient photoinduced charge separation reactions are central to the performance of natural photosynthetic systems and to emerging technologies for renewable energy production, including both bulk heterojunction devices[1] and systems for artificial photosynthesis.[2−5] The desired electron transfer reactions in these systems must outcompete deactivation processes to avoid dissipating captured energy as waste heat.[1−6] For example, in the reaction center of purple nonsulfur bacteria, excitation of a special pair of bacteriochlorophyll molecules, P865, initiates rapid electron transfer to a nearby bacteriopheophytin in ∼3 ps followed by charge shift to ubiquinone Q_A ($\tau \sim 200$ ps) and then to ubiquinone Q_B ($\tau \sim 200$ μs), generating a distal electron−hole pair and storing energy efficiently in a long-lived charge separated state.[7,8] Similarly tuned photoinduced charge separation and electron transfer cascades are required for high performance bulk heterojunction devices[1,6,9] and artificial solar-to-fuel energy conversion.[2−5]

Quantitatively accurate and computationally inexpensive predictions of photoinduced electron transfer reaction rates within molecular systems from first-principles could facilitate rapid, rational design of efficient materials for solar energy conversion. However, useful accuracy with inexpensive methods remains difficult to achieve. In the nonadiabatic high-temperature or activated crossing limit, Marcus theory predicts that the rate of electron transfer is given by[10,11]

$$k_{I\to F} = \frac{2\pi}{\hbar}|H_{IF}|^2\sqrt{\frac{1}{4\pi k_B T\lambda}}\,e^{-(\lambda+\Delta G^\circ)^2/(4\lambda k_B T)} \quad (1)$$

where $k_{I\to F}$ is the rate of electron transfer from the initial state (I) to the final state (F), H_{IF} is the diabatic electronic matrix element for the coupling between the two states, λ is the reorganization energy, and ΔG° is the total free energy change between the initial and final states. For eq 1, the high temperature or activated crossing limit requires that $k_b T \gg (\hbar\omega)^2/\lambda$, where ω is the maximum frequency of any nuclear vibrational mode coupled to the electronic system.[11,12] Eq 1 also assumes that two shifted parabolas represent the free-energy surfaces for the nuclear vibrations of the initial and final states and that first-order time-dependent perturbation theory is valid for the reaction.

Recently, Subotnik et al. accurately predicted triplet−triplet energy transfer rates from biphenyl or benzophenone donors to a naphthalene acceptor across a series of rigid bridging molecules, using eq 1 in conjunction with configuration interaction singles (CIS) theory to compute ΔG°, λ, and, with a modified Boys or a Edmiston−Ruedenberg localized diabatization routine, H_{IF}.[13] Initially, we sought to extend this same methodology to computing H_{IF} for photoinduced electron transfer reactions. However, it was found that CIS systematically overestimates the vertical excitation energy of

Received: August 18, 2014
Revised: October 17, 2014
Published: October 22, 2014

DOI: 10.1021/jp508337x
J. Phys. Chem. A 2015, 119, 253−262

charge transfer (CT) states relative to non-charge transfer (non-CT) states by >1 eV.[14] This large bias against CT states, capable of reversing the experimentally observed state ordering, strongly limits the direct use of CIS theory to predict H_{IF} for photoinduced electron transfer reactions without a means to correct the relative state energies.[15] To address this problem, Subotnik and co-workers recently developed the perturbatively orbital optimized CIS (OO-CIS) method, which provides a significant correction to CT state energies by using a single Newton−Raphson step to optimize orbitals.[16] A variational extension of OO-CIS, VOA-CIS, was also developed, which can properly describe electronic structure near a crossing point.[17,18] The goal of this work is to determine the potential utility of the OO-CIS and VOA-CIS wavefunction methods for predicting electron transfer rates using eq 1.

Excited State Potential Energy Surfaces. As a means of comparison, we will benchmark OO-CIS and VOA-CIS against CIS, CIS(D), and TD-DFT. We first discuss CIS(D), a perturbative post-CIS correction, which can improve CIS energies strongly with moderate computational cost. Designed by Head-Gordon et al., CIS(D) introduces a doubles and triples correction while increasing the scaling from N^4 for CIS to N^5, where N is the number of orbitals.[19] Unfortunately, CIS(D) only provides corrected energies, not other properties. Also, because it is a perturbative method, CIS(D) is expected to fail for nearly degenerate excited states or when the energy difference between S_0 and S_1 is small. The OO-CIS method has the same limitations. In general, CC2,[20] ADC(2),[21,22] and CIS(D_n) methods[23] also scale as N^5 and should provide corrected property predictions near excited state crossings, though only the Hermitian ones will yield the right topology near a conical intersection.[24] [CIS(2) is also variational and Hermitian and should be stable near crossings.[25]] In this paper, we will restrict ourselves to comparisons with CIS(D); in the future, additional benchmarking against the other methods mentioned above would be interesting (though a bit more expensive).

Next, we turn our attention to time-dependent density functional theory (TD-DFT), which provides an alternative for computing excited state energies and properties with moderate computational cost (without relying on a wavefunction in theory). While TD-DFT has many successes in the literature, local exchange-correlation DFT functionals tend to underestimate the energy of CT states and (unlike CIS) do not exhibit the correct $-1/r$ distance-dependence for the potential energy of CT states, where r is a distance coordinate between the separated charges.[26,27] To calculate accurate CT and non-CT excited state energies,[28−31] one must employ long-range corrected (LRC) functionals, which partition the coulomb operator to include exact Hartree−Fock exchange at long-range (and thus recover the correct $-1/r$ distance dependence[30,32]). In this paper, we will benchmark the OO-CIS and VOA-CIS methods versus the cheap, long-range corrected ωB97X functional.[32]

Electronic Couplings. To compute the square of the electronic coupling, $|H_{IF}|^2$ in eq 1, a number of diabatization schemes are available,[33] including Generalized Mulliken−Hush (GMH),[34,35] Boys localization,[36,37] fragment charge difference (FCD),[38] and constrained DFT.[39−42] To apply the GMH method to a two-state problem, the dipole matrix elements of the adiabatic states $|\Phi_1\rangle$ and $|\Phi_2\rangle$ are calculated and one then focuses on $\vec{\nu}_0$, the difference between the dipole moment of the initial adiabatic state and the dipole moment of the final adiabatic state:[32,33]

$$\vec{\nu}_0 = (\vec{\mu}_{11} - \vec{\mu}_{22})/|\vec{\mu}_{11} - \vec{\mu}_{22}| \quad (2)$$

The adiabatic dipole matrix elements are projected onto $\vec{\nu}_0$, and the projected dipole matrix is diagonalized.[34,35] The rotation matrix that diagonalizes the projected dipole matrix is used as the adiabatic to diabatic transformation matrix.[34,35] Boys localization provides an extension to GMH for systems with more than two charge centers.[36] In the two-state case, Boys localization provides the same result as GMH if $\vec{\nu}_0$ and $\vec{\mu}_{12}$ are parallel or antiparallel.[36]

While this paper will use GMH and Boys localization to calculate diabatic couplings, it is worthwhile to highlight how these methods differ from the other popular diabatization techniques listed above. Similar to Boys localization, the fragment charge difference method can model ET systems while accounting for multiple charge centers. FCD forms diabats from adiabats by maximizing charge separation between diabats; however, the method requires a priori assignment of donor and acceptor fragments so as to measure charge locality.[38] Finally, constrained density functional theory (CDFT) is a very different approach from GMH or Boys localization. CDFT constructs diabatic states directly (without first forming adiabats) by insisting that various molecular fragments have predetermined charges. Thus, similar to the fragment charge difference method, CDFT requires a priori assignment of donor and acceptor groups, which may be problematic for donor and acceptor fragments that are not spatially well-separated.[39−42] Constrained density functional theory is also limited to the calculation of the electronic coupling between the ground state and the lowest energy charge transfer state or the electronic coupling between charge localized states in a mixed valence system.[42] As a result, CDFT does not apply easily to the computation of electronic coupling for photoinduced charge separation reactions (which is the focus of this article).[42]

Outline. In the end, this paper will address the potential utility of the OO-CIS and VOA-CIS wavefunction methods for predicting electron transfer rates by quantifying their ability to predict the relative energies of non-CT and CT states and the square of the electronic coupling, $|H_{IF}|^2$, between such states for a series of six small donor−acceptor dyads. Following the work of Pasman et al.,[43] a perturbative approach based on a spectral analysis of excitation energies and oscillator strengths is used to compute $|H_{IF}|^2$. For comparison, the GMH and Boys localization methods will also be used to compute $|H_{IF}|^2$. The results are compared with experimental values, and, as indicated above, benchmarked against CIS, CIS(D), and the LRC ωB97X functional.

The format of the remainder of this paper is as follows. In Section II, experimental reference data reported by Pasman et al.[43] for the six donor−acceptor dyads is presented. Additionally, the experimental methods[43] used to estimate the energy difference and square of the electronic coupling between the CT and non-CT states for each dyad are reviewed. In Section III, the computational methods are described. In Section IV, the computational results are presented and evaluated in terms of how well each method predicts the experimental values. Conclusions are given in Section V.

DOI: 10.1021/jp508337x
J. Phys. Chem. A 2015, 119, 253−262

II. EXPERIMENTAL REFERENCE DATA

Over 30 years ago, Pasman and co-workers reported the absorption spectra of the small molecule donor−acceptor dyads **1b−1c** and **6a−6d** and the corresponding acceptor-only molecules **11b−11c** and **10a−10d** (Figure 1) in *n*-hexanes at

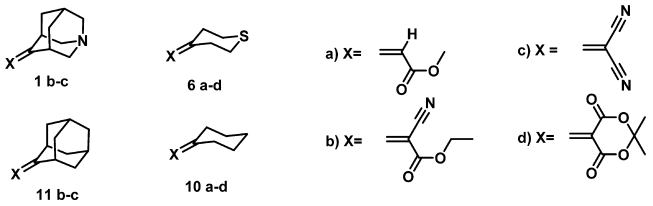

Figure 1. Molecules considered in this study. Molecules **1b−1c** and **6a−6d** have both donor and acceptor groups and exhibit low-energy CT and non-CT transitions. Molecules **11b−11c** and **10a−10d** are corresponding reference compounds without donor groups that exhibit a single dominant low-energy non-CT transition.

20 °C.[43] For each of the small molecule donor−acceptor dyads, there are two low-lying electronic transitions with significant oscillator strength.[43] Conversely, in each acceptor-only molecule, a single dominant transition occurs at slightly lower energy than the high-energy transition in the corresponding dyad with an intensity approximately equal to the sum of the two low-lying transitions for the dyad.[43] On the basis of these observations, the lower-energy transition, observed only in the dyads, has been assigned to the formation of a CT state and the higher-energy transition, observed in both the dyads and acceptor-only molecules, to the formation of a non-CT state resulting primarily from local $\pi \rightarrow \pi^*$ excitation of the acceptor group.[43]

For the donor−acceptor dyads **1b−1c** and **6a−6d**, the energy difference $\Delta E = E_{\text{non-CT}} - E_{\text{CT}}$ and the square of the electronic coupling, $|H_{\text{IF}}|^2$, between the observed CT and non-CT states were estimated experimentally (Table 1).[43] Specifically, ΔE was determined by using the λ_{max} of the observed transitions in the donor−acceptor dyads to approximate the excitation energies.[43] For each dyad, $|H_{\text{IF}}|^2$ was estimated using eq 3 below, which can be derived using first-order perturbation theory:[44]

$$\frac{\varepsilon_{\text{CT}}}{\varepsilon_{\text{non-CT}}} = \frac{|H_{\text{IF}}|^2}{(2E_{\text{Ref}} - E_{\text{non-CT}} - E_{\text{CT}})^2} \quad (3)$$

where ε_{CT} is the extinction coefficient of the CT transition, $\varepsilon_{\text{non-CT}}$ is the extinction coefficient of the non-CT transition, E_{ref} is the energy of the non-CT excited state in the corresponding acceptor-only compound, $E_{\text{non-CT}}$ is the energy of the non-CT excited state in the donor−acceptor dyad, and E_{CT} is the energy of the charge transfer excited state in the donor−acceptor dyad.[43]

III. METHODS

General. All calculations were performed with the 6-31G* basis set using Q-Chem 3.2 or later and, for VOA-CIS, a modified developer version of Q-Chem.[45] Because the reference data was collected in *n*-hexanes, solvent effects (e.g., significant solvent stabilization of CT states) are expected to be minimal and no solvent model was used. Moreover, it is of interest to determine if the OO-CIS and VOA-CIS methods can provide accurate results using a moderately sized basis set and no solvation as these conditions would allow for comparatively fast candidate screening for solar energy conversion applications.

Geometry Optimization. Optimized ground state geometries were obtained using both the MP2 method and the ωB97X functional. For **6a−6d** and **10a−10d**, the chair conformation was used based on the reported similarity of the spectra of **6b** and **6c** to analogous molecules (see **5b** and **5c**)[43] constrained by a fused ring to the chair conformation. Frequency calculations confirmed the absence of imaginary modes for each optimized geometry.

Excited State Calculations. MP2 optimized geometries were used for CIS, CIS(D), OO-CIS, and VOA-CIS calculations. For ωB97X calculations, geometries optimized with the ωB97X functional were used. VOA-CIS was performed using the VOA-CIS-G(10,2) option and a rimp2-cc-pvdz auxiliary basis set.

IV. NUMERICAL RESULTS

State Assignments. To analyze the excited state results, a correspondence between the computed transitions and the experimentally observed CT and non-CT transitions is required. Figures 2, 3, and 4 show the transitions computed

Table 1. Energies and Extinction Coefficients of Non-CT and CT Transitions, ΔE, and $|H_{\text{IF}}|^2$ for 1b−1c and 6a−6d.[43] Energies and Extinction Coefficients of Non-CT Transitions for 11b−11c and 10a−10d.[43]

molecule	non-CT (eV)	non-CT ε (M^{-1} cm^{-1})	CT (eV)	CT ε (M^{-1} cm^{-1})	ΔE (eV)	$\lvert H_{\text{IF}}\rvert^2$ (eV^2)[a]
1b	5.42	8780	3.92	4900	1.50	0.46
1c	5.44	8300	3.91	4500	1.54	0.43
6a	5.90	15700	4.88	2920	1.02	0.066
6b	5.44	10000	4.36	2100	1.08	0.13
6c	5.44	13500	4.28	2860	1.17	0.17
6d	5.39	9870	4.08	1910	1.31	0.19
11b	5.12	14400	–	–	–	–
11c	5.12	12000	–	–	–	–
10a	5.69	15400	–	–	–	–
10b	5.29	14700	–	–	–	–
10c	5.31	18200	–	–	–	–
10d	5.23	10000	–	–	–	–

[a]These values are calculated using eq 3 with the reported energies and extinction coefficients. Adapted with permission from ref 43. Copyright 1982 American Chemical Society.

DOI: 10.1021/jp508337x
J. Phys. Chem. A 2015, 119, 253−262

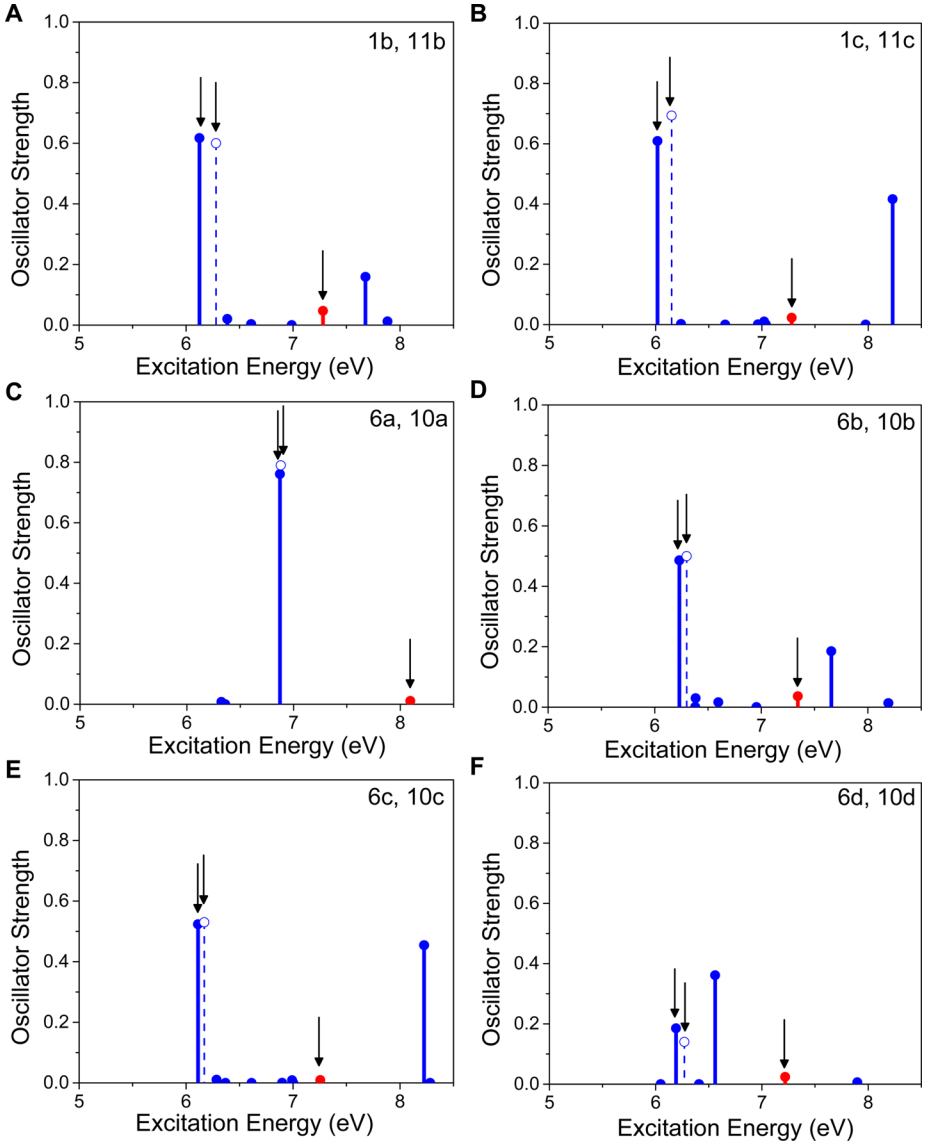

Figure 2. Excitation energies and oscillator strengths for **1b**−**1c** and **6a**−**6d** calculated using CIS are plotted in (A−F), respectively, for excitation energies < 8.5 eV. Red indicates CT states ($|\vec{\mu}_{rel}| \geq 2.1$ au). Solid blue indicates non-CT states ($|\vec{\mu}_{rel}| < 2.1$ au). Arrows identify the dominant low-energy CT and non-CT transitions assigned to the experimentally observed transitions. The non-CT transition for acceptor-only molecules **11b**−**11c** and **10a**−**10d** calculated with CIS are shown in (A−F), respectively, as empty blue circles with dashed blue lines.

using CIS (up to 8.5 eV), VOA-CIS (up to 7.5 eV), and ωB97X (up to 7.5 eV), respectively. To aid identification, states with a relative dipole moment, $|\vec{\mu}_{rel}| = |\vec{\mu}_{ex} - \vec{\mu}_{gs}|$, greater than or equal to 2.1 au are assigned as CT states (red), while states with $|\vec{\mu}_{rel}| < 2.1$ au are assigned as non-CT states (blue).

For each dyad, CIS predicts a single CT state below 8.5 eV. This transition is assigned to the experimentally observed CT transition. For **1b**−**1c** and **6a**−**6c**, there is a single dominant low-energy non-CT transition which is assigned to the experimentally observed non-CT transition. CIS predicts two strong non-CT transitions in the 6−7 eV range with oscillator strengths >0.18 for **6d**. The lower-energy transition is assigned to the lowest energy experimentally observed non-CT transition. Since OO-CIS and CIS(D) are perturbative methods that correct the CIS energies, the same state assignments were made for OO-CIS and CIS(D).

For each dyad, VOA-CIS predicts a single low-energy CT state, which is readily assigned to the experimentally observed CT state. For **1c**, **6a**, **6c**, and **6d**, there is a single dominant low-energy (<7.5 eV) non-CT transition that is assigned to the experimentally observed non-CT transition. VOA-CIS predicts two non-CT transitions with oscillator strengths >0.05 at energies below 7 eV for **1b** and **6b**. In each case, the higher-energy transition is assigned to the experimentally observed non-CT transition based on the significantly higher oscillator strengths of these transitions, which are commensurate with the high experimentally observed extinction coefficients (ε = 8780 M^{-1} cm^{-1} and ε = 10000 M^{-1} cm^{-1}, respectively, Table 1). Confirming these assignments, dominant non-CT transitions at similar energies were computed for reference molecules **11b** and **10b** (vide infra).

As in VOA-CIS, for each dyad ωB97X predicts a single low-energy CT state that is assigned to the experimentally observed CT state. For **1c** and **6a**−**6d**, there is a single dominant low-energy (<7.5 eV) non-CT transition that is assigned to the experimentally observed non-CT transition. ωB97X predicts

DOI: 10.1021/jp508337x
J. Phys. Chem. A 2015, 119, 253−262

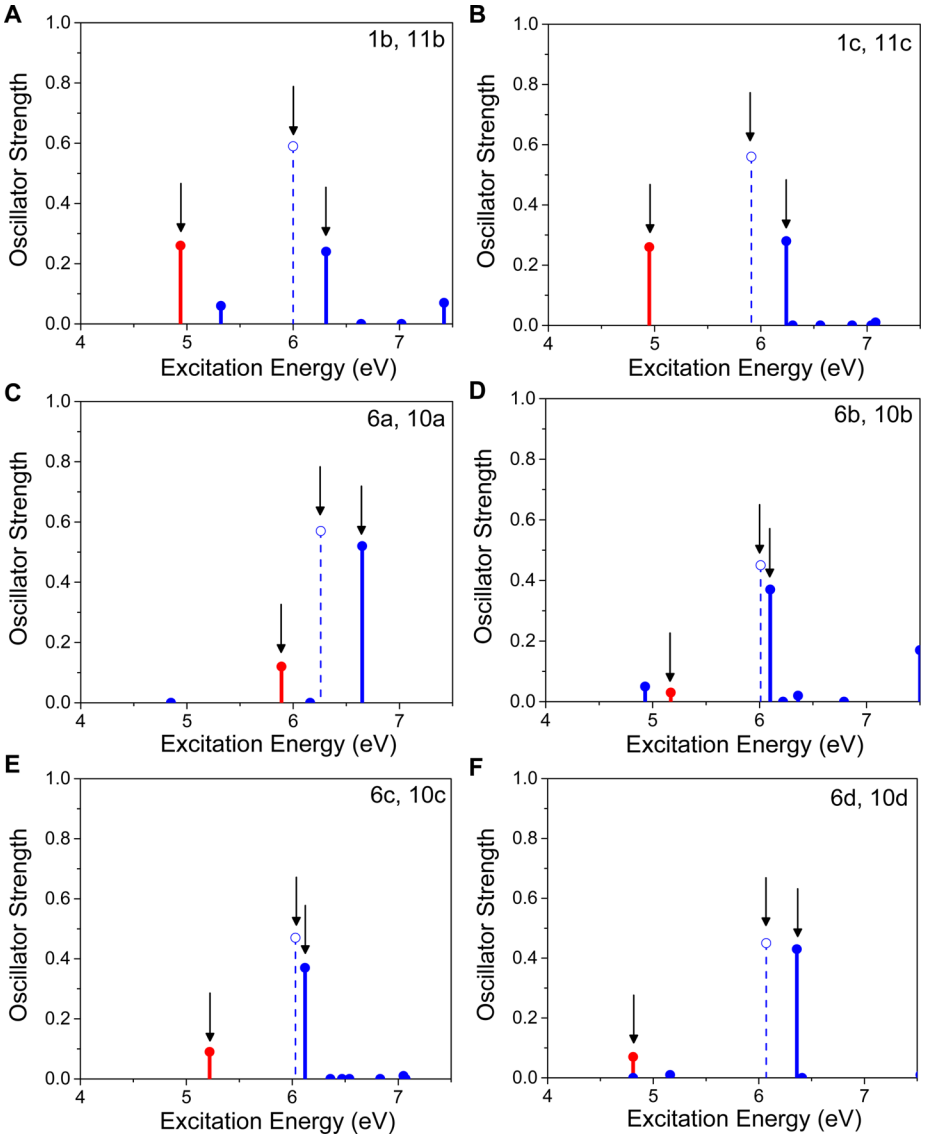

Figure 3. Excitation energies and oscillator strengths for **1b**−**1c** and **6a**−**6d** calculated using VOA-CIS are plotted in (A−F), respectively, for excitation energies < 7.5 eV. Red indicates CT states ($|\vec{\mu}_{rel}| \geq 2.1$ au). Solid blue indicates non-CT states ($|\vec{\mu}_{rel}| < 2.1$ au). Arrows identify the dominant low-energy CT and non-CT transitions assigned to the experimentally observed transitions. The non-CT transition for acceptor-only molecules **11b**−**11c** and **10a**−**10d** calculated with VOA-CIS are shown in (A−F), respectively, as empty blue circles with dashed blue lines.

two non-CT transitions in the 5−7 eV range with oscillator strengths >0.05 for **1b**. As described above for VOA-CIS, the higher-energy transition is assigned to the experimentally observed transition on the basis of its significantly higher oscillator strength and a computed dominant non-CT transition at a similar energy for **11b** (vide infra).

Among the computed transitions for reference molecules **11b**−**11c** and **10a**−**10d**, the experimentally observed non-CT transition can be identified based on its oscillator strength and energy relative to the non-CT transition identified in each dyad. The assigned transitions are shown for CIS, VOA-CIS, and ωB97X in Figures 2−4, respectively, as blue empty circles with dashed lines. Specifically, CIS theory predicts for each reference molecule that the lowest-energy transition with nonzero oscillator strength is a strong non-CT transition (oscillator strength >0.14) with an excitation energy similar to that computed for the non-CT transition in each respective dyad. These transitions are assigned as the experimentally observed non-CT transitions in the reference molecules. The same state assignments are made for OO-CIS and CIS(D). For each reference molecule, VOA-CIS predicts a single strong non-CT transition (oscillator strength >0.45) at energies <7.4 eV with all other transitions in this energy range having oscillator strengths <0.03. Each of these strong transitions is assigned to the corresponding experimentally observed non-CT transition. Similar to VOA-CIS, for each reference molecule ωB97X predicts a single strong non-CT transition (oscillator strength > 0.54) at energies < 7.5 eV, with all other transitions in this energy range having oscillator strengths <0.04. Each strong transition is assigned to the respective experimentally observed non-CT transition.

Computed versus Experimental ΔE. With the use of the states assignments and the computed excitation energies shown in Figures 2−4, the predicted ΔE values for each method were determined. Figure 5 plots these calculated values versus the experimental ΔE values (Table 1). Figure 6 displays the root mean squared error (RMSE) for each method. For each dyad, CIS inverts the experimentally observed state ordering

DOI: 10.1021/jp508337x
J. Phys. Chem. A 2015, 119, 253−262

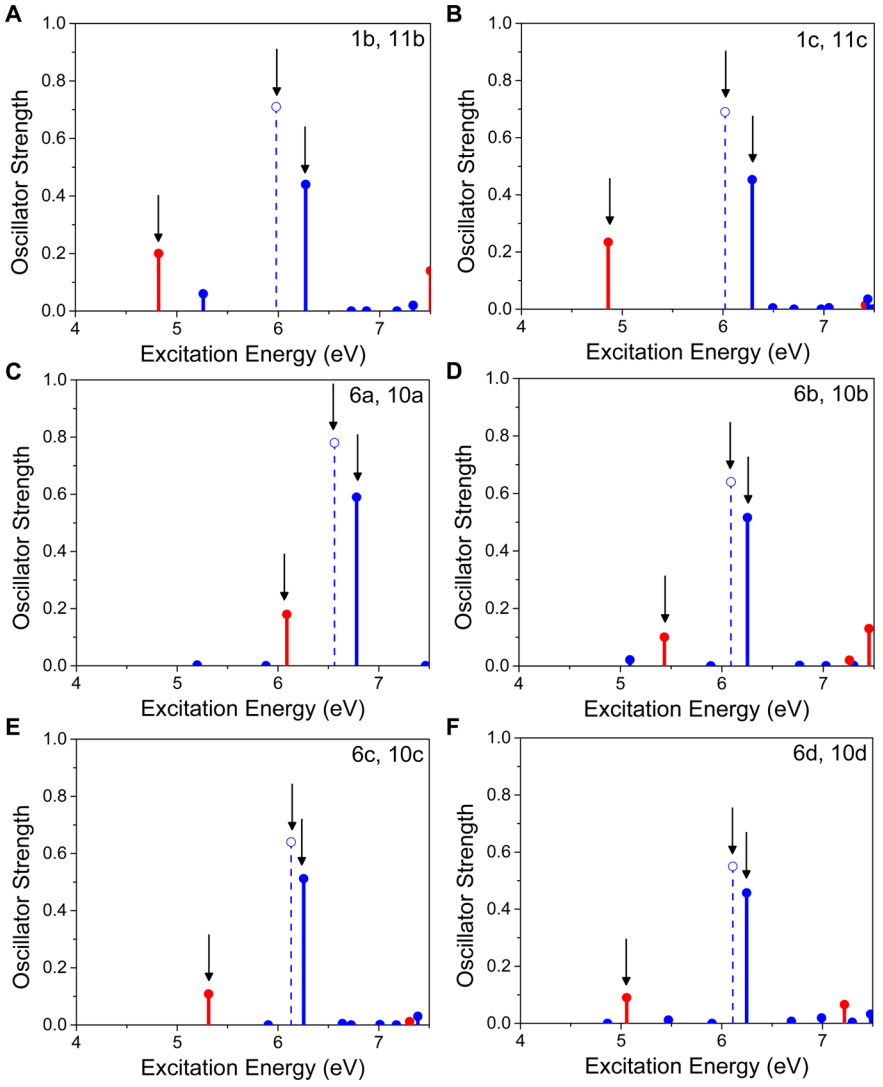

Figure 4. Excitation energies and oscillator strengths for **1b−1c** and **6a−6d** calculated using ωB97X are plotted in (A−F), respectively, for excitation energies < 7.5 eV. Red indicates CT states ($|\vec{\mu}_{rel}| \geq 2.1$ au). Solid blue indicates non-CT states ($|\vec{\mu}_{rel}| < 2.1$ au). Arrows identify the dominant low-energy CT and non-CT transitions assigned to the experimentally observed transitions. The non-CT transition for acceptor-only molecules **11b−11c** and **10a−10d** calculated with ωB97X are shown in (A−F), respectively, as empty blue circles with dashed blue lines.

(calculated $\Delta E < 0$) and produces errors in excess of 2.1 eV (RMSE = 2.43 eV). OO-CIS gives a significant energy correction to the CT states sufficient to recover the correct state ordering for **6c** and **6d**; however, OO-CIS still underestimates ΔE by at least 0.8 eV for each dyad with RMSE = 1.54 eV. CIS(D) is consistently more accurate than OO-CIS with a RMSE of 1.12 eV, however, it also fails to predict the experimentally observed trend. VOA-CIS and ωB97X have nearly equivalent RMSE of 0.22 eV and 0.21 eV, respectively. Qualitatively, VOA-CIS follows the experimental trend as shown by the linear least-squares fit (blue line) in Figure 5. However, the uncertainty in the slope and intercept are large with estimated values of 1.1 ± 0.4 and −0.3 ± 0.5 (value ± standard error), respectively, and $R^2 = 0.64$. The ΔE values computed with ωB97X also qualitatively predict the experimental trend as shown by the linear least-squares fit (light blue dashed line) in Figure 5. The ωB97X values show less deviation from a linear fit with corresponding slope and intercept estimates of 1.46 ± 0.07 and −0.8 ± 0.1 (value ± standard error), respectively, and $R^2 = 0.99$.

Computed versus Experimental $|H_{IF}|^2$. Using the computed energies and oscillator strengths for the non-CT and CT transitions in each dyad, **1b−1c** and **6a−6d**, as well as the computed energy of the non-CT transition in the corresponding reference molecules, **11b−11c** and **10a−10d**, eq 3 was used to compute $|H_{IF}|^2$ between the non-CT and CT state in each dyad, substituting the computed oscillator strengths for extinction coefficients. The resulting values for each computational method are plotted in Figure 7 versus the experimental $|H_{IF}|^2$ values from Table 1. The RMSE for each computational method is graphed in Figure 6. For OO-CIS and CIS(D), which only provide corrections to the CIS energies, the CIS oscillator strengths were used to calculate the $|H_{IF}|^2$ values shown.

CIS, OO-CIS, and CIS(D) all provide inaccurate electronic coupling with RMSE values of 0.24 eV^2, 0.28 eV^2, and 0.23 eV^2, respectively. This result is unsurprising given that CIS consistently underestimates the oscillator strength of the CT transition relative to the oscillator strength of the non-CT transition and CIS, OO-CIS, and CIS(D) all incorrectly predict

DOI: 10.1021/jp508337x
J. Phys. Chem. A 2015, 119, 253−262

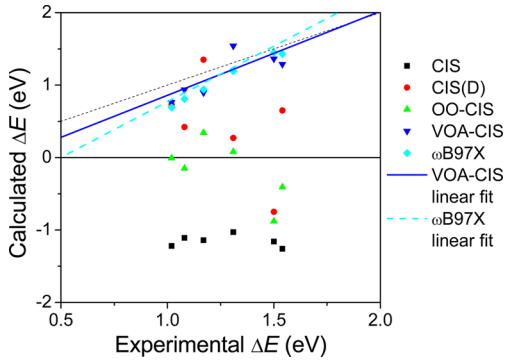

Figure 5. Calculated ΔE values using each method are plotted for **1b**−**1c** and **6a**−**6d** and compared with the experimental values. For reference, the dashed line shows an exact match between calculated and experimental values. Linear least-squares fits to the ΔE values computed using VOA-CIS (slope = 1.1 ± 0.4, vertical axis intercept = −0.3 ± 0.5, reported as value ± standard error, R^2 = 0.64) and ωB97X (slope = 1.46 ± 0.07, vertical axis intercept = −0.8 ± 0.1, reported as value ± standard error, R^2 = 0.99) are shown as blue continuous and light blue dashed lines, respectively.

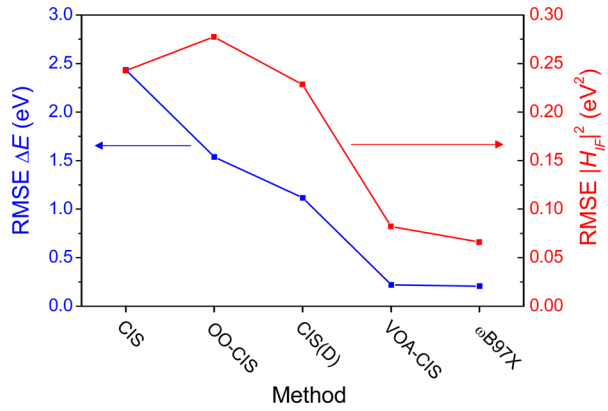

Figure 6. Root mean squared error for the computed ΔE values and the $|H_{IF}|^2$ values computed using eq 3 for **1b**−**1c** and **6a**−**6d**.

the relative energies of these transitions. Conversely, VOA-CIS and ωB97X both reliably predict the experimentally determined $|H_{IF}|^2$ values with RMSE values of only 0.08 eV^2 and 0.07 eV^2, respectively.[46] In comparison to CIS, VOA-CIS and especially ωB97X more closely reproduce the experimentally observed $\varepsilon_{CT}/\varepsilon_{non\text{-}CT}$ ratio. VOA-CIS and ωB97X also both predict the oscillator strength of the non-CT transition in the reference molecule to be approximately equal to the sum of the CT and non-CT transitions in each corresponding dyad, as observed experimentally. For VOA-CIS and ωB97X, the computed oscillator strength ratios combined with the accuracy of the computed relative transition energies result in accurate predictions of $|H_{IF}|^2$ using eq 3. Linear least-squares fits of $|H_{IF}|^2$ values computed with VOA-CIS and ωB97X are shown in Figure 7. Both VOA-CIS and ωB97X correctly predict the experimental trend in $|H_{IF}|^2$ values with ωB97X slightly outperforming VOA-CIS in this regard. For VOA-CIS and ωB97X, respectively, the estimates ± the standard error for the slopes are 1.3 ± 0.2 and 1.0 ± 0.1, while the corresponding vertical axis intercepts are −0.10 ± 0.06 and −0.05 ± 0.03.

For comparison, $|H_{IF}|^2$ values were computed for each dyad using the GMH algorithm of Cave and Newton[34,35] with CIS, VOA-CIS, and ωB97X (Table 2). The $|H_{IF}|^2$ values for VOA-CIS were also computed using Boys localization.[36,37] The Boys

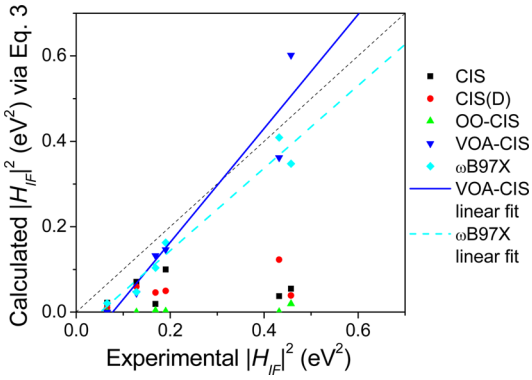

Figure 7. $|H_{IF}|^2$ values calculated using eq 3 (with oscillator strengths substituted for extinction coefficients). Computational values from a variety of different electronic structure methods are plotted for **1b**−**1c** and **6a**−**6d** versus the experimental values. For reference, the dashed line shows an exact match between calculated and experimental values. Linear least-squares fits to the $|H_{IF}|^2$ values computed using VOA-CIS (slope =1.3 ± 0.2, vertical axis intercept = −0.10 ± 0.06, reported as value ± standard error, R^2 = 0.91) and ωB97X (slope = 1.0 ± 0.1, vertical axis intercept = −0.05 ± 0.03, reported as value ± standard error, R^2 = 0.96) are shown as blue continuous and light blue dashed lines, respectively.

Table 2. Calculated Values of $|H_{IF}|^2$ (eV^2) Obtained Using Generalized Mulliken−Hush Theory with CIS, VOA-CIS, and ωB97X for 1b−1c and 6a−6d, Root Mean Squared Error vs. the Experimental Values, and Sample Correlation Coefficients for Comparisons Among CIS, VOA-CIS, and ωB97X Methods

molecule	CIS	VOA-CIS	ωB97X
1a	0.24	0.38	0.28
1b	0.19	0.24	0.22
6a	0.066	0.057	0.068
6b	0.084	0.079	0.070
6c	0.053	0.052	0.064
6d	0.077	0.13	0.13
RMSE vs Experimental:	0.15	0.10	0.13
Sample correlation with			
CIS	1	–	–
VOA-CIS	0.98	1	–
ωB97X	0.97	0.99	1

localization results differed from the GMH results by less than 0.0033 eV^2 for each dyad. For the dyads considered, this indicates the validity of the GMH approximation that the important direction is the one defined by $\vec{v}_0$ (eq 2). Figure 8 plots the $|H_{IF}|^2$ values computed with GMH versus the experimental values from Table 1. For VOA-CIS and ωB97X, the $|H_{IF}|^2$ values calculated using GMH show greater deviation from the experimental values than those computed with eq 3. While some of this disagreement could reflect limitations of the GMH and Boys methods, this disagreement could also very likely be due to errors in the experimental estimates from eq 3. After all, eq 3 assumes that $|H_{IF}|^2$ should be small but $|H_{IF}|^2$ is relatively large for the dyads considered here, and the magnitude of the electronic coupling estimated experimentally with eq 3 approaches ΔE.

Finally, we end this discussion by mentioning a peculiarity. For each dyad, the $|H_{IF}|^2$ values calculated via GMH theory

DOI: 10.1021/jp508337x
J. Phys. Chem. A 2015, 119, 253−262

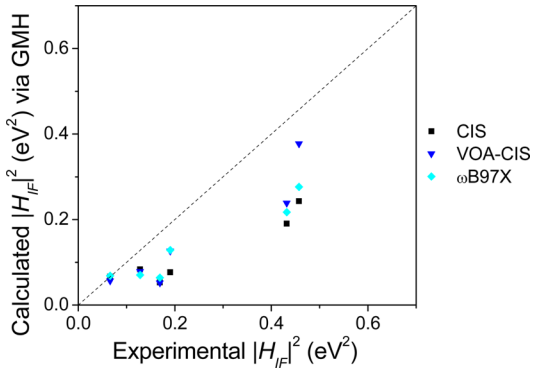

Figure 8. $|H_{IF}|^2$ values computed using Generalized Mulliken–Hush with CIS, VOA-CIS, and ωB97X are plotted versus the experimental values for **1b–1c** and **6a–6d**.

using CIS, VOA-CIS, and ωB97X are very similar as evidenced by (i) the sample correlation coefficients that approach one for each pair of methods (Table 2) and (ii) the graph in Figure 9,

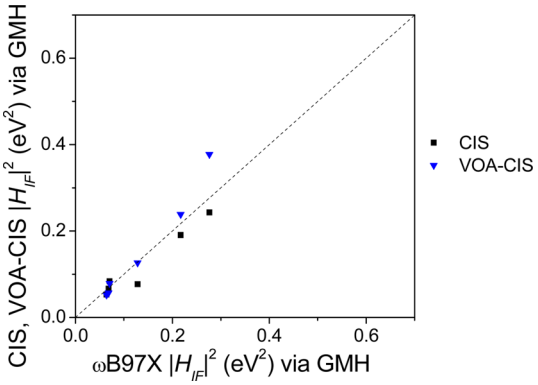

Figure 9. $|H_{IF}|^2$ values computed using Generalized Mulliken–Hush with CIS and VOA-CIS are plotted versus the values computed with ωB97X for **1b–1c** and **6a–6d**.

which shows the $|H_{IF}|^2$ values computed using GMH for CIS and VOA-CIS versus the values computed with ωB97X. Given that, for each dyad, VOA-CIS and ωB97X produce similar ΔE values and $|H_{IF}|^2$ values via eq 3, it is perhaps not surprising that the $|H_{IF}|^2$ values calculated via GMH theory would also be similar. However, it is not immediately clear why CIS, which fails to predict the same state ordering and gives markedly different $|H_{IF}|^2$ values via eq 3, should produce such similar $|H_{IF}|^2$ values via GMH theory. This result may be related to a recent observation from Cave and Newton, which suggests that $|H_{IF}|^2$ values calculated via GMH theory should be insensitive to errors in diabatic state energies.[47] Nonetheless, further investigation is warranted to determine if $|H_{IF}|^2$ values calculated with GMH theory using CIS versus VOA-CIS and ωB97X methods consistently correlate despite large differences between the predicted state energies.

V. CONCLUSION

Using Marcus theory to predict rates of photoinduced electron transfer reactions with sufficient accuracy to guide detailed molecular design requires accurate computational methods for predicting the relative energies of non-CT and CT states as well as the electronic coupling between these states. This work shows that OO-CIS and CIS(D), two perturbative corrections to CIS theory, while a significant improvement over CIS, do not provide this required accuracy nor do they reliably make qualitative predictions of trends in the relative energies or electronic coupling between non-CT and CT states. That being said, VOA-CIS, which combines the doubles contributions incorporated in CIS(D) theory and orbital optimization used in OO-CIS,[17,18] provides not only qualitative predictions of trends but also nearly quantitative accuracy in predicting the energy differences and electronic coupling between non-CT and CT states. Remarkably, VOA-CIS accomplishes this with no parametrization based on experimental data, providing accuracy roughly on par with that achieved with the ωB97X functional. Although parametrized with experimental data, the performance of ωB97X in reproducing the experimental ΔE and $|H_{IF}|^2$ values is notable here, especially since excitation energies were not fit during the parametrization.[32] Other functionals that were parametrized to reproduce experimental excitation energies, including LRC-ωPBEh, may offer further accuracy improvements.[28] In regard to VOA-CIS, since the memory requirements are moderate and the algorithm is highly parallelizable,[17,18] it may prove to be a useful tool for guiding the rational design of efficient charge-separating materials for solar energy conversion technologies. Once a parallelized implementation is ready, further study should be undertaken to assess the performance of VOA-CIS for predicting electron transfer rates in larger donor–bridge–acceptor systems and in the limit of weaker electronic coupling than that exhibited by the small donor–acceptor dyads studied in this work.

AUTHOR INFORMATION

Corresponding Author

*E-mail: ratner@northwestern.edu.

Notes

The authors declare no competing financial interest.

ACKNOWLEDGMENTS

B.S.V. was supported by the Department of Energy Office of Science Graduate Fellowship Program (DOE SCGF), made possible in part by the American Recovery and Reinvestment Act of 2009, administered by ORISE-ORAU under contract DE-AC05-06OR23100. M.R.W. is supported by the Chemical Sciences, Geosciences, and Biosciences Division, Office of Basic Energy Sciences, DOE under grant DE-FG02-99ER14999. M.A.R. was supported by the ANSER Center, an Energy Frontier Research Center funded by the U.S. Department of Energy, Office of Science, Office of Basic Energy Sciences, under Award DE-SC0001059. M.A.R. thanks the Israel/US Science Foundation (BSF) for support, Grant 2011509. J.E.S. and X.L. were supported by NSF CAREER Grant CHE-1150851. J.E.S. acknowledges an Alfred P. Sloan Research Fellowship and a David & Lucile Packard Fellowship.

REFERENCES

(1) Brédas, J.-L.; Norton, J. E.; Cornil, J.; Coropceanu, V. Molecular Understanding of Organic Solar Cells: The Challenges. *Acc. Chem. Res.* **2009**, *42*, 1691–1699.

(2) Moore, G. F.; Brudvig, G. W. Energy Conversion in Photosynthesis: A Paradigm for Solar Fuel Production. *Annu. Rev. Condens. Matter Phys.* **2011**, *2*, 303–327.

(3) Alstrum-Acevedo, J. H.; Brennaman, M. K.; Meyer, T. J. Chemical Approaches to Artificial Photosynthesis. 2. *Inorg. Chem.* **2005**, *44*, 6802–6827.

DOI: 10.1021/jp508337x
J. Phys. Chem. A 2015, 119, 253–262

(4) Gust, D.; Moore, T. A.; Moore, A. L. Solar Fuels via Artificial Photosynthesis. *Acc. Chem. Res.* **2009**, *42*, 1890−1898.
(5) Wasielewski, M. R. Energy, Charge, and Spin Transport in Molecules and Self-Assembled Nanostructures Inspired by Photosynthesis. *J. Org. Chem.* **2006**, *71*, 5051−5066.
(6) Servaites, J. D.; Savoie, B. M.; Brink, J. B.; Marks, T. J.; Ratner, M. A. Modeling Geminate Pair Dissociation in Organic Solar Cells: High Power Conversion Efficiencies Achieved with Moderate Optical Bandgaps. *Energy Environ. Sci.* **2012**, *5*, 8343−8350.
(7) Blankenship, R. E. *Molecular Mechanisms of Photosynthesis*; Blackwell Science: Oxford, 2002.
(8) Woodbury, N. W.; Allen, J. P. In *Anoxygenic Photosynthetic Bacteria*; Blankenship, R. E., Madigan, M. T., Bauer, C. E., Eds.; Kluwer Academic Publishers: Dordrecht, The Netherlands, 1995; pp 527−557.
(9) Ohkita, H.; Cook, S.; Astuti, Y.; Duffy, W.; Tierney, S.; Zhang, W.; Heeney, M.; McCulloch, I.; Nelson, J.; Bradley, D. D. C.; et al. Charge Carrier Formation in Polythiophene/Fullerene Blend Films Studied by Transient Absorption Spectroscopy. *J. Am. Chem. Soc.* **2008**, *130*, 3030−3042.
(10) Marcus, R. A. The Theory of Oxidation-Reduction Reactions Involving Electron Transfer. I. *J. Chem. Phys.* **1956**, *24*, 966−978.
(11) Schatz, G. C.; Ratner, M. A. *Quantum Mechanics in Chemistry*; Prentice-Hall, Inc.: Englewood Cliffs, NJ, 1993.
(12) Jortner, J. Temperature Dependent Activation Energy for Electron Transfer Between Biological Molecules. *J. Chem. Phys.* **1976**, *64*, 4860−4867.
(13) Subotnik, J. E.; Vura-Weis, J.; Sodt, A. J.; Ratner, M. A. Predicting Accurate Electronic Excitation Transfer Rates via Marcus Theory with Boys or Edmiston−Ruedenberg Localized Diabatization. *J. Phys. Chem. A* **2010**, *114*, 8665−8675.
(14) Subotnik, J. E. Communication: Configuration Interaction Singles Has a Large Systematic Bias Against Charge-Transfer States. *J. Chem. Phys.* **2011**, *135*, 071104.
(15) Chen, H.-C.; Hsu, C.-P. Ab Initio Characterization of Electron Transfer Coupling in Photoinduced Systems: Generalized Mulliken−-Hush with Configuration-Interaction Singles. *J. Phys. Chem. A* **2005**, *109*, 11989−11995.
(16) Liu, X.; Fatehi, S.; Shao, Y.; Veldkamp, B. S.; Subotnik, J. E. Communication: Adjusting Charge Transfer State Energies for Configuration Interaction Singles: Without any Parameterization and with Minimal Cost. *J. Chem. Phys.* **2012**, *136*, 161101.
(17) Liu, X.; Ou, Q.; Alguire, E.; Subotnik, J. E. Communication: An Inexpensive, Variational, Almost Black-Box, Almost Size-Consistent Correction to Configuration Interaction Singles for Valence Excited States. *J. Chem. Phys.* **2013**, *138*, 221105.
(18) Liu, X.; Subotnik, J. E. The Variationally Obital-Adapted Configuration Interaction Singles (VOA-CIS) Approach to Electronically Excited States. *J. Chem. Theory Comput.* **2014**, *10*, 1004−1020.
(19) Head-Gordon, M.; Rico, R. J.; Oumi, M.; Lee, T. J. A Doubles Correction to Electronic Excited States from Configuration Interaction in the Space of Single Substitutions. *Chem. Phys. Lett.* **1994**, *219*, 21−29.
(20) Christiansen, O.; Koch, H.; Jørgensen, P. The Second-Order Approximate Coupled Cluster Singles and Doubles Model CC2. *Chem. Phys. Lett.* **1995**, *243*, 409−418.
(21) Schirmer, J. Beyond the Random-Phase Approximation: A New Approximation Scheme for the Polarization Propagator. *Phys. Rev. A* **1982**, *26*, 2395−2416.
(22) Starcke, J. H.; Wormit, M.; Dreuw, A. Unrestricted Algebraic Diagrammatic Construction Scheme of Second Order for the Calculation of Excited States of Medium-Sized and Large Molecules. *J. Chem. Phys.* **2009**, *130*, 024104.
(23) Head-Gordon, M.; Oumi, M.; Maurice, D. Quasidegenerate Second-Order Perturbation Corrections to Single-Excitation Configuration Interaction. *Mol. Phys.* **1999**, *96*, 593−602.
(24) Krylov, A. I. Equation-of-Motion Coupled-Cluster Methods for Open-Shell and Electronically Excited Species: The Hitchhiker's Guide to Fock Space. *Annu. Rev. Phys. Chem.* **2008**, *59*, 433−462.
(25) Laikov, D.; Matsika, S. Inclusion of Second-Order Correlation Effects for the Ground and Singly-Excited States Suitable for the Study of Conical Intersections: The CIS(2) Model. *Chem. Phys. Lett.* **2007**, *448*, 132−137.
(26) Dreuw, A.; Weisman, J. L.; Head-Gordon, M. Long-Range Charge-Transfer Excited States in Time-Dependent Density Functional Theory Require Non-Local Exchange. *J. Chem. Phys.* **2003**, *119*, 2943−2946.
(27) Dreuw, A.; Head-Gordon, M. Failure of Time-Dependent Density Functional Theory for Long-Range Charge-Transfer Excited States: The Zincbacteriochlorin−Bacteriochlorin and Bacteriochlorophyll−Spheroidene Complexes. *J. Am. Chem. Soc.* **2004**, *126*, 4007−4016.
(28) Rohrdanz, M. A.; Martins, K. M.; Herbert, J. M. A Long-Range-Corrected Density Functional That Performs Well for Both Ground-State Properties and Time-Dependent Density Functional Theory Excitation Energies, Including Charge-Transfer Excited States. *J. Chem. Phys.* **2009**, *130*, 054112.
(29) Rohrdanz, M. A.; Herbert, J. M. Simultaneous Benchmarking of Ground- and Excited-State Properties with Long-Range-Corrected Density Functional Theory. *J. Chem. Phys.* **2008**, *129*, 034107.
(30) Tawada, Y.; Tsuneda, T.; Yanagisawa, S.; Yanai, T.; Hirao, K. A Long-Range-Corrected Time-Dependent Density Functional Theory. *J. Chem. Phys.* **2004**, *120*, 8425−8433.
(31) Yanai, T.; Tew, D. P.; Handy, N. C. A New Hybrid Exchange-Correlation Functional Using the Coulomb-Attenuating Method (CAM-B3LYP). *Chem. Phys. Lett.* **2004**, *393*, 51−57.
(32) Chai, J.-D.; Head-Gordon, M. Systematic Optimization of Long-Range Corrected Hybrid Density Functionals. *J. Chem. Phys.* **2008**, *128*, 084106.
(33) Hsu, C.-P. The Electronic Couplings in Electron Transfer and Excitation Energy Transfer. *Acc. Chem. Res.* **2009**, *42*, 509−518.
(34) Cave, R. J.; Newton, M. D. Generalization of the Mulliken−Hush Treatment for the Calculation of Electron Transfer Matrix Elements. *Chem. Phys. Lett.* **1996**, *249*, 15−19.
(35) Cave, R. J.; Newton, M. D. Calculation of Electronic Coupling Matrix Elements for Ground and Excited State Electron Transfer Reactions: Comparison of the Generalized Mulliken−Hush and Block Diagonalization Methods. *J. Chem. Phys.* **1997**, *106*, 9213−9226.
(36) Subotnik, J. E.; Yeganeh, S.; Cave, R. J.; Ratner, M. A. Constructing Diabatic States from Adiabatic States: Extending Generalized Mulliken−Hush to Multiple Charge Centers with Boys Localization. *J. Chem. Phys.* **2008**, *129*, 244101.
(37) Subotnik, J. E.; Cave, R. J.; Steele, R. P.; Shenvi, N. The Initial and Final States of Electron and Energy Transfer Processes: Diabatization as Motivated by System-Solvent Interactions. *J. Chem. Phys.* **2009**, *130*, 234102.
(38) Voityuk, A. A.; Rösch, N. Fragment Charge Difference Method for Estimating Donor−Acceptor Electronic Coupling: Application to DNA π-Stacks. *J. Chem. Phys.* **2002**, *117*, 5607−5616.
(39) Wu, Q.; Van Voorhis, T. Direct Optimization Method to Study Constrained Systems within Density-Functional Theory. *Phys. Rev. A* **2005**, *72*, 024502.
(40) Wu, Q.; Van Voorhis, T. Constrained Density Functional Theory and Its Application in Long-Range Electron Transfer. *J. Chem. Theory Comput.* **2006**, *2*, 765−774.
(41) Wu, Q.; Van Voorhis, T. Direct Calculation of Electron Transfer Parameters through Constrained Density Functional Theory. *J. Phys. Chem. A* **2006**, *110*, 9212−9218.
(42) Wu, Q.; Van Voorhis, T. Extracting Electron Transfer Coupling Elements from Constrained Density Functional Theory. *J. Chem. Phys.* **2006**, *125*, 164105.
(43) Pasman, P.; Rob, F.; Verhoeven, J. W. Intramolecular Charge-Transfer Absorption and Emission Resulting from Through-Bond Interaction in Bichromophoric Molecules. *J. Am. Chem. Soc.* **1982**, *104*, 5127−5133.
(44) Pasman, P. Ph.D. Dissertation, University of Amsterdam, 1980.
(45) Shao, Y.; Molnar, L. F.; Jung, Y.; Kussmann, J.; Ochsenfeld, C.; Brown, S. T.; Gilbert, A. T. B.; Slipchenko, L. V.; Levchenko, S. V.;

DOI: 10.1021/jp508337x
J. Phys. Chem. A 2015, 119, 253−262

O'Neill, D. P.; et al. Advances in Methods and Algorithms in a Modern Quantum Chemistry Program Package. *Phys. Chem. Chem. Phys.* **2006**, *8*, 3172−3191.

(46) The mean absolute percent error (MAPE) is another means to assess the accuracy of the $|H_{IF}|^2$ values calculated using eq 3 for **1b**−**1c** and **6a**−**6d**. In contrast to RMSE, MAPE places a signficant weight on comparatively small absolute errors if they are associated with correspondingly small $|H_{IF}|^2$ values. For underestimation, MAPE has an upper limit of 100%. There is no upper bound for overestimation. The MAPE values are 71%, 99%, 75%, 43%, and 36%, respectively, for CIS, OO-CIS, CIS(D), VOA-CIS, and ωB97X. The RMSE values follow the same trend.

(47) Cave, R. J.; Newton, M. D. Multistate Treatments of the Electronic Coupling in Donor−Bridge−Acceptor Systems: Insights and Caveats from a Simple Model. *J. Phys. Chem. A* **2014**, *118*, 7221−7234.

DOI: 10.1021/jp508337x
J. Phys. Chem. A 2015, 119, 253−262